PAPER • OPEN ACCESS

TiO$_2$, SiO$_2$, and Al$_2$O$_3$ coated nanopores and nanotubes produced by ALD in etched ion-track membranes for transport measurements

To cite this article: Anne Spende *et al* 2015 *Nanotechnology* **26** 335301

View the article online for updates and enhancements.

TiO$_2$, SiO$_2$, and Al$_2$O$_3$ coated nanopores and nanotubes produced by ALD in etched ion-track membranes for transport measurements

Anne Spende[1,2], Nicolas Sobel[3], Manuela Lukas[4], Robert Zierold[5],
Jesse C Riedl[1], Leonard Gura[1], Ina Schubert[1], Josep M Montero Moreno[5],
Kornelius Nielsch[5], Bernd Stühn[4], Christian Hess[3],
Christina Trautmann[1,2] and Maria E Toimil-Molares[1]

[1] Materialforschung, GSI Helmholtzzentrum für Schwerionenforschung, Darmstadt, Germany
[2] Material- und Geowissenschaften, Technische Universität Darmstadt, Germany
[3] Eduard-Zintl-Institut für Anorganische und Physikalische Chemie, Technische Universität Darmstadt, Germany
[4] Institut für Festkörperphysik, Technische Universität Darmstadt, Germany
[5] Institut für Nanostruktur- und Festkörperphysik, Universität Hamburg, Germany

E-mail: m.e.toimilmolares@gsi.de and A.Spende@gsi.de

Abstract

Low-temperature atomic layer deposition (ALD) of TiO$_2$, SiO$_2$, and Al$_2$O$_3$ was applied to modify the surface and to tailor the diameter of nanochannels in etched ion-track polycarbonate membranes. The homogeneity, conformity, and composition of the coating inside the nanochannels are investigated for different channel diameters (18–55 nm) and film thicknesses (5–22 nm). Small angle x-ray scattering before and after ALD demonstrates conformal coating along the full channel length. X-ray photoelectron spectroscopy and energy dispersive x-ray spectroscopy provide evidence of nearly stoichiometric composition of the different coatings. By wet-chemical methods, the ALD-deposited film is released from the supporting polymer templates providing 30 μm long self-supporting nanotubes with walls as thin as 5 nm. Electrolytic ion-conductivity measurements provide proof-of-concept that combining ALD coating with ion-track nanotechnology offers promising perspectives for single-pore applications by controlled shrinking of an oversized pore to a preferred smaller diameter and fine-tuning of the chemical and physical nature of the inner channel surface.

Keywords: ion-track technology, atomic layer deposition, single-pore, polycarbonate membrane, ion transport, nanotubes

(Some figures may appear in colour only in the online journal)

1. Introduction

Synthetic nanochannels integrated in solid state membranes are of high relevance for basic research and industrial application in various fields including nanofluidics, filtration, catalysis, and sensorics. In the recent past, membranes containing only one individual nanochannel have gained special attention as biomimicking model systems for cell membranes, single-molecule sensors, and devices for molecular recognition [1–4]. If the channel diameter is comparable to the size of a given macromolecule, the passage of a single molecule through the nanochannel can be monitored by resistive-pulse

sensing [5–7]. The blocking of the ion current across the membrane is registered as a discrete electrical signal. To study transport processes of e.g., water [8], drugs [9], or macromolecules such as DNA in nanoconfinements, nanochannels with few nm inner diameter are required.

In the past, several approaches have been developed for efficient and reproducible fabrication of single solid-state nanochannels including ion beam and electron beam sculpturing, lithography, and etching [10]. Many of these techniques are restricted to specific materials and/or provide limited flexibility in adjusting the channel length and diameter in a controlled manner. To this day, producing solid-state nanopores with diameters below 10 nm remains a challenge. Several methods begin with a larger channel and reduce the channel size in a second step, e.g., by deposition of material in the channel [11, 12] or shrinking the channel by electron beam exposure [13].

This paper describes our approach to fabricate nanochannels by ion-track nanotechnology and control the reduction of the channel size by atomic layer deposition (ALD). Because ALD is based on successive, separated, and self-terminating gas–solid surface reactions of typically two gaseous reactants, it is an ideal technique to coat complex three-dimensional topographies with a homogeneous film of known composition and thickness. The self-limiting nature of the chemical reactions ensures ultra-precise process control. Another benefit of using ALD is that even deeply embedded surfaces such as the inner wall of nanochannels with large aspect (length-to-diameter) ratios can be completely coated with a uniform film.

Ion-track technology provides nanochannels of tailored size. It is based on swift heavy ion beams available at large accelerator facilities. Polymer foils (or other insulating targets) are irradiated with a well-defined number of heavy ions of kinetic energy in the range of MeV to GeV. The beam energy is sufficiently high that the ions completely penetrate through several tens of μm thick foils. During slowing down, each ion creates a track of 5–10 nm in diameter, consisting of broken polymer chains and other defects [14–17]. The tracks are stochastically distributed over the target area but if necessary can be precisely placed on predefined positions [18]. By selectively dissolving the damaged material, each track is converted into an open nanochannel. The time and other parameters of the chemical etching process (e.g., temperature, concentration of the etchant etc.) determine the diameter of the nanochannel. The pore size can be adjusted to diameters between about 10–20 nm up to several μm [14, 19–22], whereas the production of diameters below 10 nm is difficult because the damage zone of the unetched track has already an extension of 5–10 nm. Ion-track technology is commonly applied to polymers, such as polycarbonate (PC), polyethylene terephthalate, and polyimide but also works well for selected inorganic materials (e.g., mica and quartz). Polymeric track-etched membranes are commercially available and applied as specific filters, if a small channel size distribution is important. In basic research such membranes are most suitable as templates to fabricate nanowires and nanotubes by electrochemical [22] or electroless deposition [23, 24].

Since each ion produces a track, the number of channels can be precisely controlled by the irradiation using one single ion per sample up to about 10^{10} ions per cm^2. The fact that the channel length, geometry, and diameter can be easily controlled and the possibility to adjust the channel number down to one individual nanochannel represent a great advantage compared to other nanoporous systems such as anodic aluminum oxide (AAO) membranes.

ALD coating of track-etched nanochannels is of interest because it allows us to shrink the diameter of track-etched channels in a very controlled manner without affecting the channel geometry. The deposited material can be applied to adjust specific surface properties like catalytic activity, corrosion resistance, and hydrophobicity. Moreover, surface properties of nanochannels in polymers have a strong influence on ionic transport processes. Etching PC leads for instance to charged carboxylate groups (–COO$^-$) at the inner channel wall [25]. The influence of dangling bonds and swelling on the shape of the nanochannel in solution, as well as the effect of pH variations on the effective surface charge, is not completely clear. Systematic transport studies would benefit from an inorganic reference surface.

In the recent past, ALD coatings of TiO$_2$, SiO$_2$, and Al$_2$O$_3$ were already successfully applied to different porous systems including AAO membranes [26–30]. Sander *et al* deposited TiO$_2$ layers of less than 3 nm thickness in 40 nm wide nanochannels in AAO (aspect ratio 38) [26]. Al$_2$O$_3$ coatings of AAO with an aspect ratio of 770 are described by Elam *et al* [27]. Romero *et al* coated AAO with SiO$_2$ up to an aspect ratio of 3000 and performed ionic transport measurements with NaCl in a multichannel AAO membrane [28]. Furthermore, all three oxide materials were also deposited in etched ion-track PC membranes [9, 31–36]. Aspect ratios of 300 were achieved by Bae *et al* for TiO$_2$ and Al$_2$O$_3$ [33]. Our group recently reported the deposition of SiO$_2$ in PC templates up to an aspect ratio of 1500 [36].

Here, we describe the conformal deposition of TiO$_2$, SiO$_2$, and Al$_2$O$_3$ by low temperature ALD onto the surface of PC etched ion-track membranes with 30 μm long nanochannels of diameters between 18 and 55 nm. We characterized the ALD-produced coatings with respect to thickness, morphology, and composition by various complementary techniques including scanning electron microscopy (SEM), small angle x-ray scattering (SAXS), x-ray photoelectron spectroscopy (XPS), and energy dispersive x-ray spectroscopy (EDX). The surface modification by ALD of a single nanochannel membrane is demonstrated by current–voltage measurements before and after coating.

2. Experimental section

The fabrication of ALD-coated nanoporous membranes included the following three steps (figure 1): (a) PC foils were irradiated with a well-defined number of 2-GeV Au ions. (b) By wet-chemical etching the ion tracks were converted into open nanochannels, and (c) the membranes were coated with
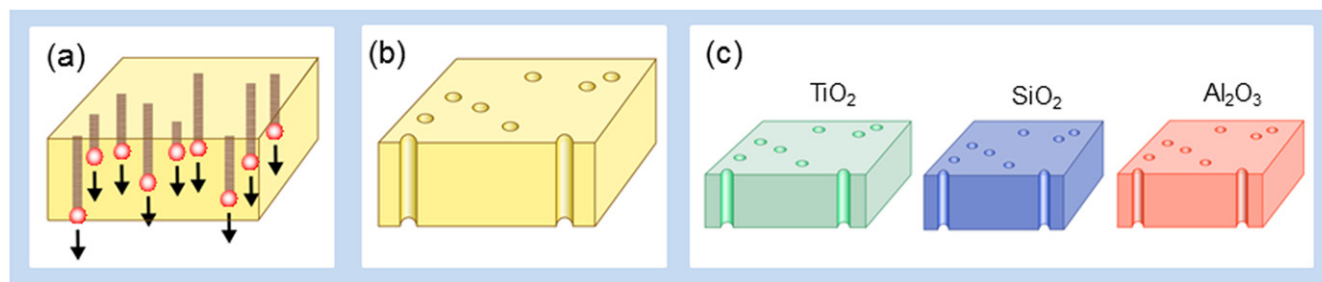
Figure 1. Scheme of fabrication of TiO_2, SiO_2, and Al_2O_3 coated track-etched membranes. (a) Polycarbonate foils are irradiated with high-energy heavy ions; each projectile creates an individual ion track; (b) chemical etching converts ion tracks into cylindrical nanochannels of well-defined diameter; (c) ALD of TiO_2, SiO_2, and Al_2O_3 produces conformal homogeneous coatings.

Table 1. Reaction mechanisms for ALD processes for TiO_2 [44], SiO_2 [45], and Al_2O_3 [27]. For SiO_2 coating, pyridine is added beforehand as a catalyst in both reaction steps. Asterisks mark reactive surface species.

	TiO_2	SiO_2	Al_2O_3
1st half reaction	$TiOH^* + Ti(OCH(CH_3)_2)_4 \rightarrow$ $TiOTi(OCH(CH_3)_2)_3{}^* + C_3H_8O$	$Si\text{-}OH^* + SiCl_4 \rightarrow$ $Si\text{–}O\text{–}SiCl_3{}^* + HCl$	$AlOH^* + Al(CH_3)_3 \rightarrow$ $AlOAl(CH_3)_2{}^* + CH_4$
2nd half reaction	$Ti(OCH(CH_3)_2)^* + H_2O \rightarrow TiOH^* + C_3H_8O$	$SiCl^* + H_2O \rightarrow$ $Si\text{–}OH^* + HCl$	$AlCH_3{}^* + H_2O \rightarrow AlOH^* + CH_4$
Reaction	$Ti(OCH(CH_3)_2)_4 + 2\ H_2O \rightarrow TiO_2 +$ $4\ C_3H_8O$	$SiCl_4 + 2$ $H_2O \rightarrow SiO_2 + 4\ HCl$	$2\ Al(CH_3)_3 + 3\ H_2O \rightarrow Al_2O_3 + 6\ CH_4$

TiO_2, SiO_2, and Al_2O_3 by applying a defined number of ALD cycles.

2.1. Ion irradiation and track etching of PC membranes

$30\ \mu m$ thick PC foils (Makrofol N, Bayer) of 3 cm in diameter were irradiated with 2-GeV Au ions at the UNILAC linear accelerator of GSI Helmholtz Centre for Heavy Ion Research (Darmstadt, Germany). The irradiation took place in vacuum and under normal beam incidence. The applied fluence was 10^9 ions cm^{-2} resulting in randomly distributed, parallel oriented ion tracks. Foils for ionic transport measurements were exposed to one single ion per sample [20, 21]. Before etching, the irradiated foils were exposed to UV light of wavelength between 280 and 400 nm for 1 h for each side. This treatment is known to reduce the size distribution of the pores during the subsequent track etching process [37–40]. Track etching was performed in 6 mol l^{-1} NaOH at 50 °C followed by rinsing in deionized water (Millipore Direct-QTMS). The etching time varied between 40 and 130 s yielding membranes with channel diameters between about 18 and 55 nm, respectively.

2.2. Atomic layer deposition

ALD was performed in different custom-built reactors (SiO_2 at Technische Universität Darmstadt [36], TiO_2 [41, 42], and Al_2O_3 at Universität Hamburg). The ALD process was conducted in stop-mode operation with an exposure-time after the precursor pulses, in which the precursor molecules can diffuse into the nanochannels. The deposition process was adjusted to temperatures below ~140 °C to avoid thermal destabilization of the PC membrane. To ensure conformal deposition of the

material along the entire $30\ \mu m$ long nanochannel, extended exposure and purge times were applied. All three materials were deposited applying purified N_2 as purge gas and water as oxygen delivering precursor.

TiO_2 was deposited at ~95 °C, using titanium isopropoxide (TTIP, SAFC Hitech). The flow rate during N_2 purge was 50 sccm. A single ALD cycle comprised (1) a pulse of 2 s of TTIP heated at 80 °C and subsequent exposure to it for 45 s, (2) 90 s of N_2 purging, (3) exposure to H_2O (pulse time 0.2 s) for 45 s, and (4) 90 s of N_2 purging.

For the deposition of SiO_2, silicon tetrachloride ($SiCl_4$, 99%, Sigma-Aldrich) and deionised H_2O were employed as precursors. Pyridine (C_5H_5N, 99.8%, anhydrous, Sigma-Aldrich) was added as catalyst to facilitate deposition at low temperature, which limited the reaction temperature to 60 °C [43]. The ALD cycle involved 5 s exposure to pyridine after a 0.1 s pulse, followed by the injection of $SiCl_4$ for 0.1 s and exposure to it for 60 s, 70 s N_2 purging at a flow rate of 200 sccm, another exposure to pyridine for 5 s (pulse time 0.1 s), and finally after a 0.1 s long pulse 60 s exposure to H_2O before another 70 s N_2 purge.

Al_2O_3 was deposited applying trimethylaluminium (TMA, SAFC Hitech) and deionised water as precursors at ~95 °C. The N_2 purging flow rate was 10 sccm. The ALD cycle consisted of 45 s TMA exposure after a TMA pulse of 0.2 s followed by 90 s N_2 purging, 45 s H_2O exposure (pulse time 0.2 s), and finally 90 s of N_2 purging.

Table 1 shows the corresponding reaction mechanisms, which can be divided into two half-reactions for all three materials. During all ALD depositions, a silicon wafer was placed in the reaction chamber as reference substrate to determine the nominal coating thickness via spectral ellipsometry.

To analyze the homogeneity and conformity of the different ALD coatings, a systematic series of etched ion-track membranes with ten different channel diameters between 18 and 55 nm was prepared. Identical starting conditions for the TiO$_2$, SiO$_2$, and Al$_2$O$_3$ process were obtained by splitting a membrane of a given channel size into several sections and expose them to the different ALD coatings. Systematic tests with respect to channel size variation and fixed ALD layer thickness were performed by placing five samples of different nanochannel diameters in the ALD reactor and coating them simultaneously. A nominal 5 nm thick layer of TiO$_2$, SiO$_2$, and Al$_2$O$_3$ required 125, 28, and 30 ALD cycles, respectively.

2.3. Scanning electron microscopy and energy dispersive x-ray diffraction

To investigate the conformity, homogeneity, and thickness of the ALD coating inside the nanochannels, the PC templates were dissolved in dichloromethane (>99.5%, Carl Roth GmbH). The released nanotubes were collected on a standard Cu transmission electron microscopy grid with lacey carbon support film and inspected by a high-resolution scanning electron microscope (JEOL JSM-7401F) equipped with a transmission electron detector (STEM-in-SEM) at 20 kV. The elemental composition of the nanotubes was studied by EDX applying a XFlash 5030 EDX Spectrometer by Bruker and a voltage of 20 kV.

2.4. Small angle x-ray scattering

ALD-coated ion-track membranes were analyzed by SAXS where the parallel oriented nanochannels are embedded in the PC matrix and act as scattering objects. SAXS provides information about the mean size and size distribution of a large channel ensemble (in our case ~10^6 nanochannels). SAXS measurements were performed on a laboratory instrument with a sealed x-ray tube (Panalytical) using Cu-K$_\alpha$ radiation ($\lambda = 1.54$ Å) and a multilayer x-ray mirror. The samples were mounted on a goniometer-like holder, allowing the rotation of the sample around two axes perpendicular to the incoming x-ray beam with an accuracy of better than 0.01°. At 150 cm distance from the sample a two-dimensional detector (Molecular Metrology) recorded the scattering pattern. The set-up provides access to the scattering vector **q** ($q = \frac{4\pi}{\lambda} \sin\theta$, with 2θ denoting the scattering angle) between 0.008 Å^{-1} and 0.25 Å^{-1}. During a SAXS measurement, the surface normal of the membrane is first oriented parallel to the incoming beam ($\gamma = 0°$) in such a way that the beam is collinear to the longitudinal axis of the parallel aligned nanochannels. Under this condition, the resulting scattering pattern on the detector consists of concentric rings caused by diffraction from the circular aperture of the nanochannels. Because of the large aspect ratio of the nanochannels, a slight tilt of the sample with respect to the x-ray beam (e.g. $\gamma = 20°$) leads to a highly anisotropic scattering pattern, consisting of a narrow streak parallel to the axis of rotation [46]. The scattered intensity, $I(\mathbf{q})$, along the streak is analyzed as a function of the scattering vector **q**. It contains information on the electron density distribution within the channel. As essential parameters the diameter of the nanochannels and the thickness of layers on its wall is deduced by fitting the $I(\mathbf{q})$ data with a model function for the form factor. It describes the nanochannels as hollow cylinders with a wall embedded in a PC matrix and computes the two-dimensional scattering pattern. As form factor we used a cylinder model as described by Engel *et al* [46] and extended it by an additional cylindrical shell to account for the ALD layer deposited on the inner pore wall. The analysis of the SAXS data considers parameters such as polydispersity of cylinder radius, electron density of the wall as well as instrumental resolution and background [46, 47].

2.5. X-ray photoelectron spectroscopy

The composition of the deposited ALD layers at the membrane surface was analyzed by XPS using a SSX 100 ESCA Spectrometer (Surface Science Laboratories Inc.) with a monochromatic Al-K$_\alpha$ source. Detail and survey spectra of TiO$_2$ and Al$_2$O$_3$ samples were measured under an angle of 45° with respect to the surface normal with a step size of the binding energy of 0.1 and 0.5 eV, respectively. Samples coated with SiO$_2$ were investigated earlier with a Mg-K$_\alpha$ source under normal beam incidence [36]. To prevent charging of the samples, the spot size of the x-ray beam (~0.25×1 mm^2) was smaller than the sample area and an electron flood gun with 0.5 eV was used. All spectra were referenced to the main C1s component at 284.5 eV. The applied relative sensitivity factors (RSF) are given in table 4. The least-square fitting analysis was performed using a Voigt function (30% Gauss fraction) and a Shirley type background.

2.6. Conductivity measurements on single nanochannels

To test ionic transport properties of ALD-coated nanochannels, membranes containing one single nanochannel were investigated by ionic conductivity measurements. In our set-up, the single-channel membrane separates two compartments of a cell filled with 1 M KCl solution (specific conductivity $\kappa = 10$ S m^{-1} at 20 °C) [16]. Using a picoammeter/voltage source (Keithley 6487), current–voltage-curves were recorded by applying various voltages between ±1 V across the membrane. For cylindrical channels, the diameter d is calculated according to $d = 2*\sqrt{\frac{I*L}{U*\kappa*\pi}}$, with I being the measured electric current, U the applied voltage, L the length of the channel, and κ the electrical conductivity of the electrolyte [16]. To avoid surface charging effects, the uncoated single channel was analyzed at pH 5, whereas for the coated channel, the KCl solution was adjusted to pH 1.9 by adding HCl. This reduced pH value corresponds to the isoelectric point of SiO$_2$-coated PC. The influence of pH on the electrolyte concentration of 1 M is insignificant.
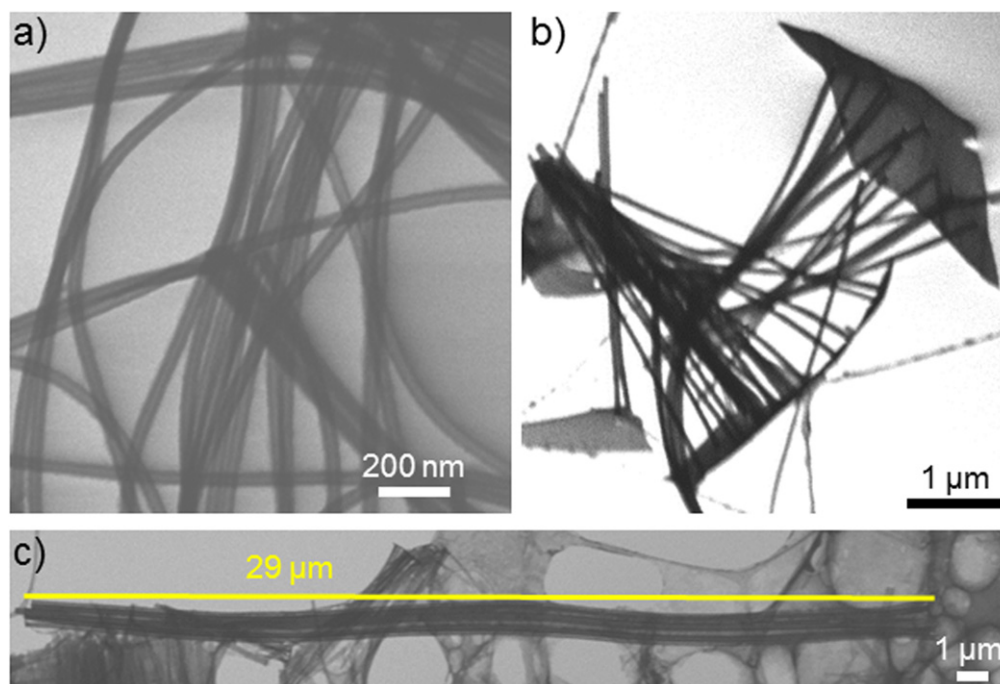
Figure 2. (a) Flexible SiO$_2$ nanotubes exhibiting an outer diameter of ∼50 nm and a wall thickness of ∼20 nm. (b) Al$_2$O$_3$ nanotubes (outer diameter ∼50 nm, wall thickness ∼15 nm), which are broken due to their rather high brittleness. They are attached to the flat Al$_2$O$_3$-film deposited on the polycarbonate surface. (c) TiO$_2$ nanotubes (outer diameter ∼100 nm due to 240 s of etching time, wall thickness ∼10 nm) with a length corresponding to the template thickness.

3. Results and discussion

3.1. Morphology and conformity of ALD coating

Figure 2 shows nanotubes of each material visualized by STEM after dissolution of the PC template. The SiO$_2$ nanotubes easily bend (a) and seem to be highly flexible, whereas most of the Al$_2$O$_3$ tubes are broken (b) indicating rather high brittleness. Image (c) shows TiO$_2$ nanotubes of 29 μm length, which corresponds to the thickness of the template. In contrast to SiO$_2$, unbroken tubes are rarely found for TiO$_2$ and Al$_2$O$_3$. This is interesting, because the fracture toughness of bulk TiO$_2$ and Al$_2$O$_3$ is about four times higher than the one of SiO$_2$.

For the quantitative analysis of the tube walls, representative STEM images of nanotube sections of all three materials are displayed in figures 3(a)–(c). At all analyzed positions along the nanotube the wall thickness of the tubes is in excellent agreement with the film thickness of the flat silicon reference sample analyzed by ellipsometry. Moreover, the respective wall thickness is independent from the initial diameter of the nanochannels. The mean diameter and wall thickness of 10–15 nanotubes of each sample are summarized in table 2. In addition, figures 3(d)–(f) display tube diameters from STEM measurements and SAXS analysis for the same samples before and after ALD coating as a function of the etching time (corresponding to different channel diameters).

The SAXS diameters are deduced from the scattering pattern, which has the shape of a narrow streak, when the sample is measured under a tilting angle of 20° (figure 3(g)). The scattered intensity, $I(\mathbf{q})$, along the streak as a function of

the scattering vector $\mathbf{q}$ as well as the corresponding fit is shown in figure 3(g) for the 90 s etched TiO$_2$-coated sample. For SiO$_2$ and Al$_2$O$_3$, the scattered intensities are shown in the insets of figures 3(e) and (f), respectively. The fact that the analysis for all samples provides an excellent fit to the scattering data demonstrates that track-etched channels are of cylindrical geometry, well aligned and with a size distribution <3% as demonstrated earlier [36, 39, 46]. The diameter of the track-etched channels increases linearly with increasing etching time [47]. After ALD deposition, the typical intensity oscillations in the SAXS spectra are preserved but shifted to larger $\mathbf{q}$ values as expected for smaller channel diameters. The scattering patterns are well described with the model of a cylindrical channel with a wall of constant electron density and thus show that the ALD deposition process is highly conformal along the full length of the channel. The determined polydispersity of the cylinder diameter is constant around 10% and does not change with coating. For the case of Al$_2$O$_3$, deviation at small q occurred, which is not understood so far. For some samples the diameters of coated channels determined by SAXS are slightly larger than the STEM data, but overall the analysis by these two techniques show good agreement. The fact that the STEM and SAXS channel diameters coincide well with the nominal coating thickness is an indication that the chosen parameters of the ALD process are suitable with respect to purging and providing sufficient exposure time for the reaction between the precursor and the surface.

To test the linearity of the ALD process in nanochannels, we systematically varied the number of ALD cycles and
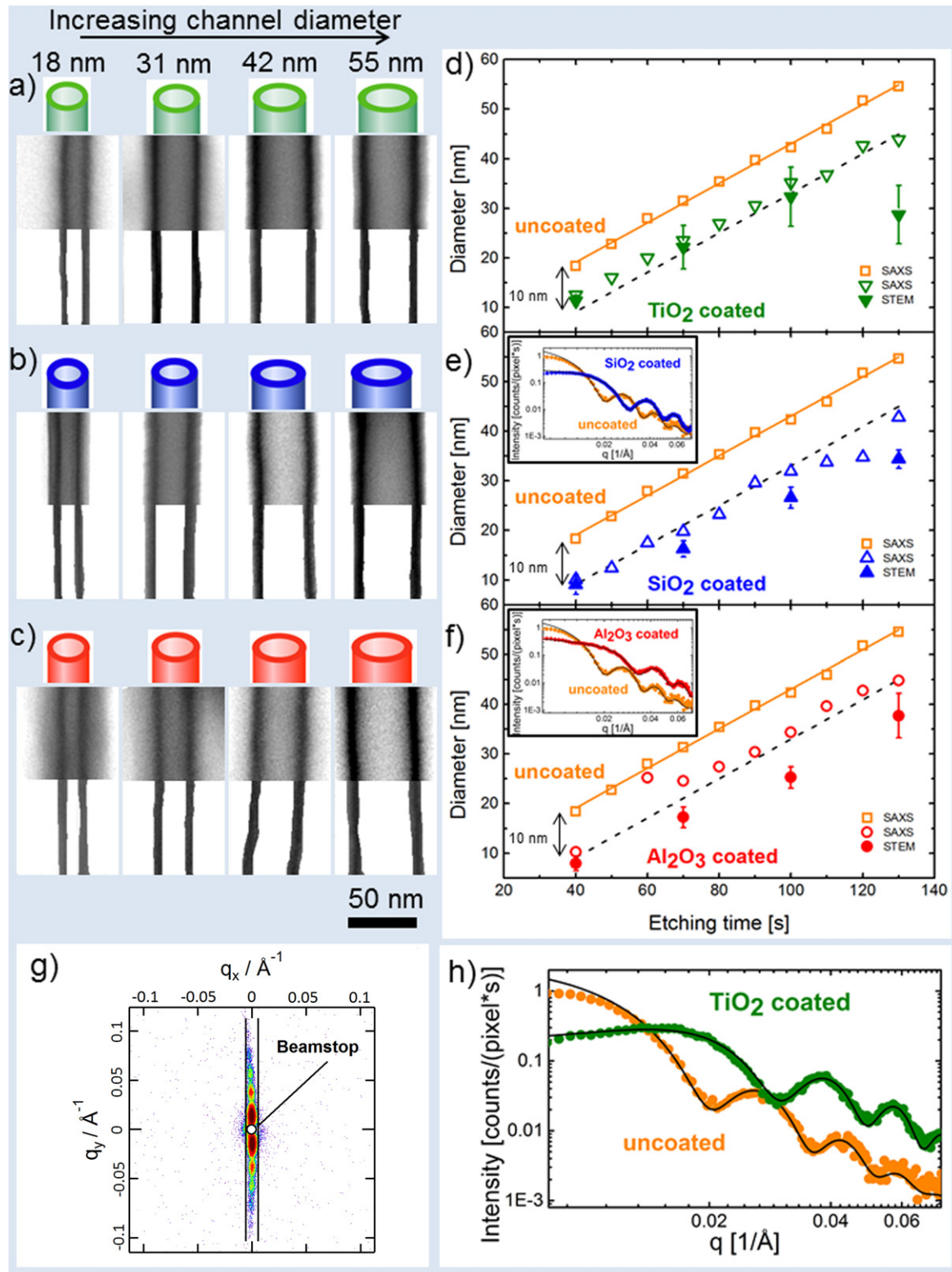
Figure 3. STEM images of single nanotubes synthesized by ALD coating of polycarbonate nanochannels with a nominal wall thickness of 5 nm of (a) TiO_2, (b) SiO_2, and (c) Al_2O_3. The outer diameters of the nanotubes are about 18, 31, 42, and 55 nm. For better visibility of the tube walls, the contrast of the lower part of the STEM images was maximized. (d), (e), (f) show the corresponding channel diameter together with results from SAXS analysis before and after ALD coating. The uncertainties of the SAXS analysis are about 0.2 nm and thus smaller than the data symbols. Solid lines are linear fits to the SAXS diameters for uncoated channels; dashed lines are guides to the eye for the reduced diameters as expected from the nominal thickness of the ALD coating. (g) The scattering pattern of the TiO_2 coated 90 s etched sample under a tilting angle of 20°. (h) and the insets of (e) and (f) display SAXS intensity oscillations before and after ALD of 90 s etched samples ($d = 40$ nm).

Table 2. Thickness of different ALD layers deduced from STEM-in-SEM images of nanotubes and from SAXS analysis before and after ALD coating with a nominal thickness of 5 nm. The uncertainty of the SAXS analysis is about ±0.2 nm. The large uncertainties of the STEM data are due to the calculation of the layer thickness by subtraction of the inner diameter from the outer diameter and the resulting error propagation.

| | Layer thickness (nm) | | | | | |
| | TiO_2 | | SiO_2 | | Al_2O_3 | |
Outer channel diameter (nm)	STEM	SAXS	STEM	SAXS	STEM	SAXS
18	4 ± 2	2.9 ± 0.21	4 ± 3	4.1 ± 0.11	5 ± 2	4.1 ± 0.26
31	6 ± 6	3.9 ± 0.24	5 ± 3	5.8 ± 0.10	6 ± 4	3.4 ± 0.20
42	4 ± 15	3.6 ± 0.22	5 ± 4	5.2 ± 0.13	6 ± 3	4 ± 0.50
55	6 ± 9	5.3 ± 0.13	5 ± 3	5.9 ± 0.18	6 ± 7	4.9 ± 0.16
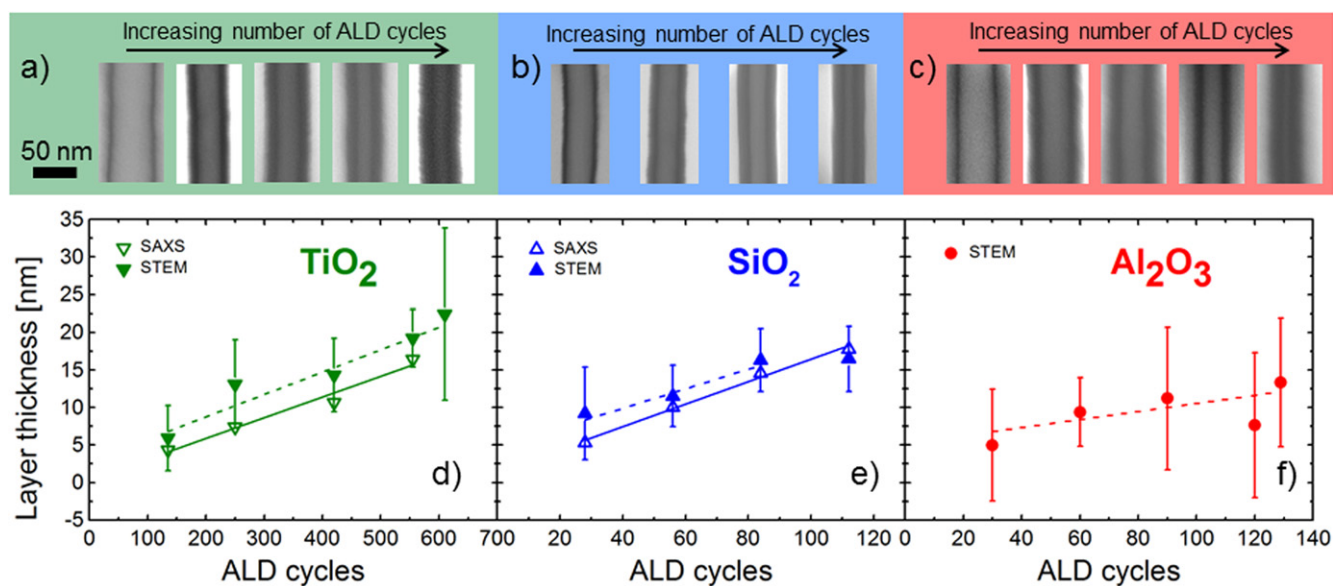
Figure 4. Series of STEM images for nanotubes of (a) TiO_2, (b) SiO_2 [36], and (c) Al_2O_3 fabricated by ALD. (d), (e), (f) show the corresponding thickness of the tube wall deduced from SAXS and STEM. The thickness of the deposited film increases linearly with the number of ALD cycles. Solid and dashed lines are linear fits to the respective SAXS and STEM data. Error bars represent the standard deviation of the nanotube analysis by STEM.

deposited 5, 10, 15, 20, and 22 nm thick layers in membranes with initial channel diameter of ∼50 nm. Depending on the material of choice, this required a different number of ALD cycles. Figure 4 displays representative STEM images of parts of the resulting nanotubes after dissolution of the PC templates. The inner diameter clearly decreases with increasing number of ALD cycles. Both, outer and inner diameter, measured at different positions along the nanotubes are constant along their entire length, evidencing a conformal deposition inside the high aspect-ratio nanochannels even for the largest film thicknesses. SAXS data of the Al_2O_3 layers are not shown because fits to the scattered intensity did not converge. This problem possibly indicates an inhomogeneous coating over a larger sample area, although the morphology and the amount of tubes transferred to the TEM grids was alike for all three materials, demonstrating conformal coating of a significant amount of nanochannels for Al_2O_3, too.

The wall thickness from STEM and SAXS analysis shows a linear dependence on the number of ALD cycles (figures 4(d)–(f)). For all three materials, maximum coating

Table 3. Layer thickness deduced from STEM-in-SEM images and SAXS analysis for different amounts of ALD cycles according to various nominal coating thicknesses. Due to experimental limitations of the SAXS system, the thickest TiO_2 coating (22 nm, 610 ALD cycles) could not be measured. For Al_2O_3 layers, the SAXS data are not shown because fits to the scattering intensity did not converge.

| | Layer thickness (nm) | | | | |
| Nominal coating (nm) | TiO_2 | | SiO_2 | | Al_2O_3 |
	STEM	SAXS	STEM	SAXS	STEM
5	6 ± 4	4.3	9 ± 6	5.3	5 ± 7
10	13 ± 6	7.4	12 ± 4	10.0	9 ± 5
15	14 ± 5	10.7	16 ± 4	14.6	11 ± 10
20	19 ± 4	16.5	16 ± 4	17.8	8 ± 10
22	22 ± 11	n.a.	—	—	13 ± 9

resulted in channels of inner diameter that are smaller than 10 nm corresponding to an aspect ratio larger than 3000. The deposition rate (slope of curve) strongly depends on the material being ∼0.03 nm/cycle for TiO_2, ∼0.15 nm/cycle for

Table 4. Surface composition (in at%) of nominal 5 and 10 nm thick TiO_2, SiO_2, and Al_2O_3 layers and pristine polycarbonate. RSF denotes the relative sensitivity factors and [*M*] stands for the respective element Ti, Si, or Al.

	Thickness (nm)	C1s[a]	O1s	Ti2p$_{3/2}$[b]	Ti–OH	Al2p	Si2p	Ratio O/[*M*]
RSF		1 (0.25)[c]	2.93 (0.66)[c]	5.22	2.93	0.537	(0.27)[c]	
TiO_2	10.9	0.21	0.45	0.2	0.14	—	—	2.25
TiO_2	5.4	0.19	0.49	0.2	0.12	—	—	2.45
SiO_2	10.0	0.12[c]	0.6[c]	—		—	0.28[c]	2.14
SiO_2	5.3	0.22[c]	0.56[c]	—		—	0.22[c]	2.54
Al_2O_3	9.6	0.10	0.59	—		0.32	—	1.84
Al_2O_3	4.8	0.13	0.58	—		0.3	—	1.93
PC	—	0.83[c]	0.17[c]	—		—	—	—

[a] Including ubiquitous carbon and carbonate species.
[b] Including Ti^{4+} and Ti^{3+} species.
[c] Values taken from Sobel *et al* [36].

SiO_2, and ~0.05 nm/cycle for Al_2O_3. Compared to the flat Si-wafer reference, the growth rate in the nanopores of TiO_2 and SiO_2 are slightly smaller, in the case of Al_2O_3 the deviation is by a factor of almost 3. The smaller growth rate of Al_2O_3 inside the nanochannels may be caused by diffusion limitations during the deposition process and can probably be avoided by further optimizing the exposure and purging times of the ALD process. The complete data set of the STEM and SAXS analysis is comprised in table 3.

3.2. Composition analysis

The surface compositions of the ALD coatings were characterized on the membrane surface by XPS, since the signal of the released nanotubes themselves was too low for a quantitative analysis. Table 4 presents the results for the different ALD layers of nominal thicknesses 5 and 10 nm (precise thickness values as determined by ellipsometry are listed) as well as for a pristine PC membrane. The calculation of the ratio between the respective O1s to Ti2p$_{3/2}$, Al2p, and Si2p peaks reveals almost stoichiometric bulk compositions for the thicker films.

Detail spectra of Ti2p, Al2p, Si2p, and the corresponding O1s peaks of 10 nm thick layers are displayed in figure 5. The spectra in figure 5(a) provide evidence of the formation of TiO_2, because of the dominance of the Ti^{4+} species with a minor contribution of Ti^{3+} of only 0.1 at% for the 5.4 nm thick layer and 0.3 at% for the 10.9 nm thick layer. The Ti2p$_{3/2}$ and Ti2p$_{1/2}$ duplets were fitted by taking into account spin–orbit coupling, and thus a 2:1 ratio of the peak areas, and a binding energy difference of $\Delta x_c = 5.65$ eV. This leads to a peak width (FWHM) that is constant for both samples. In agreement with literature [48], the binding energies of the Ti^{3+} peaks were shifted by -1.3 eV with respect to the Ti^{4+} peaks. The O1s features are assigned to Ti–O–Ti species at $\Delta x_c = 530 - 529.9$ eV and Ti–OH species at $\Delta x_c = 531.6 - 531.5$ eV [49]. The main impurity is carbon at a binding energy of 284.5 eV, which is ascribed to ubiquitous carbon (~20 at%) and a small amount of carbonate (~0.1 at%). In addition, a small amount of nitrogen impurity was detected, which may result from purging with nitrogen during ALD deposition.

Figure 5(b) present the spectra from the SiO_2 layer consisting of the Si2p peak from Si^{4+} species at a binding energy of 103.3 eV. The position of this signal and the corresponding FWHM ratio coincide with the binding energy difference (O1s–Si2p) of $\Delta x_c = 429.4$ eV and the FWHM of a native SiO_2-film on a Si-wafer [50]. Due to normal beam incidence during the XPS analysis (in contrast to tilted incidence for TiO_2 and Al_2O_3), the x-rays penetrate deeper into the SiO_2 samples yielding also information from the PC substrate. O1s and C1s peaks in the detail spectra of 5 nm thick SiO_2 films are thus ascribed to contributions from the PC membrane. There are no indications for chemical bonds between the PC substrate and the SiO_2 layer. Sobel *et al* [36] assume a sub-surface cluster growth, which is also mentioned in literature [51].

The spectra from the Al_2O_3 are shown in figure 5(c). In agreement with literature [52], the binding energy of the Al2p peak is positioned at $\Delta x_c \sim 457$ eV with respect to the O1s peak. During analysis the FWHM ratio of the fitted peaks was set constant. Carbon was the only detectable impurity; its amount decreases for thicker layer (~10 at% ubiquitous at 284.5 eV and 1 at% carbonate at ~288.5 eV binding energy).

Summarizing our XPS analysis, we find clear evidence that the ALD process on PC membranes produces very pure and almost stoichiometric TiO_2, Al_2O_3, and SiO_2 layers. Within the deposited layers, no PC signal is identified, demonstrating a homogeneous high-quality coating.

In addition to XPS, the compositions of the ALD layers were analyzed by characterizing the nanotubes by EDX in the SEM. Figure 6 shows integrated EDX spectra of linescans recorded across a single TiO_2 (green), SiO_2 (blue), and Al_2O_3 (red) nanotube on a Cu-lacey TEM grid. To attain significant count rates, the investigations were performed on nanotubes with thickest walls (20 nm) and outer diameters of 50 nm. The EDX spectra from the TiO_2, SiO_2, and Al_2O_3 nanotubes show the respective peaks of titanium, silicon, and aluminum. The height of the carbon peak varies depending on the position of the analyzed nanotube relative to the lacey carbon support film of the TEM grid. Nitrogen and chlorine peaks are not present for any of the three materials, evidencing a pure deposition and preparation process.
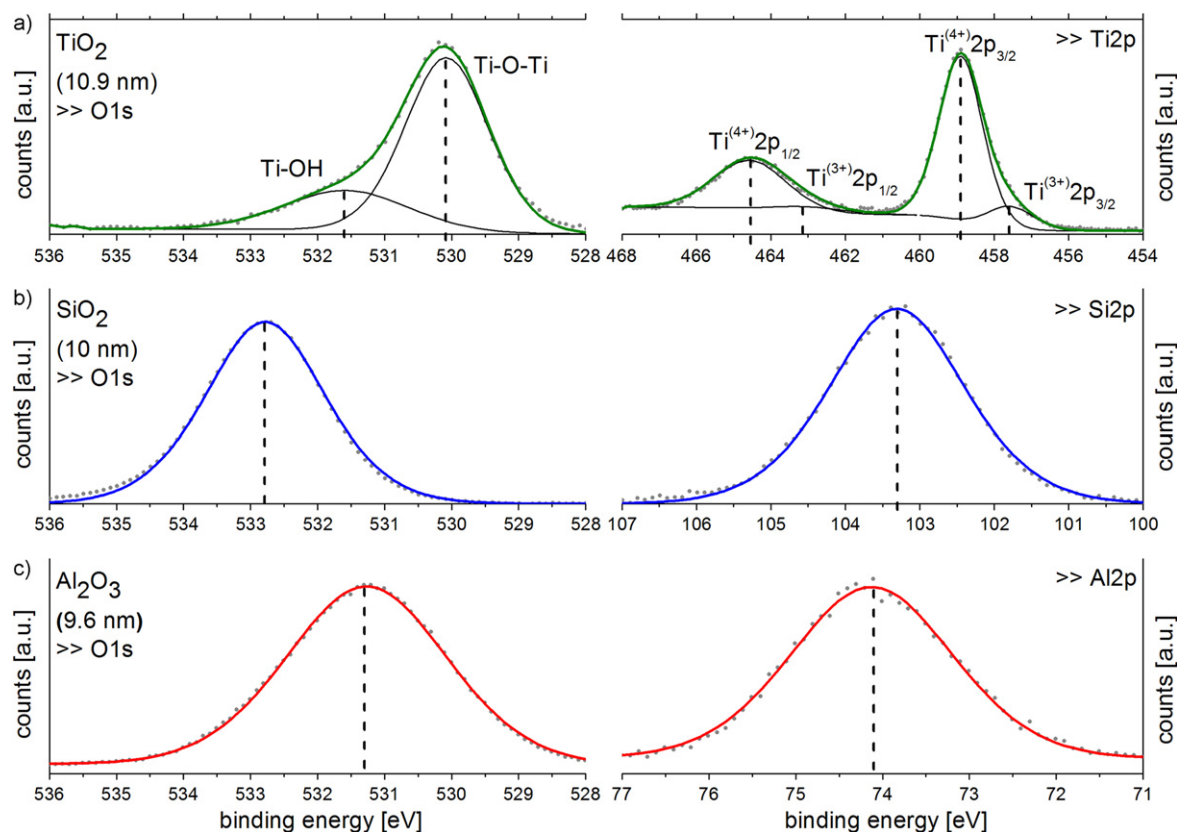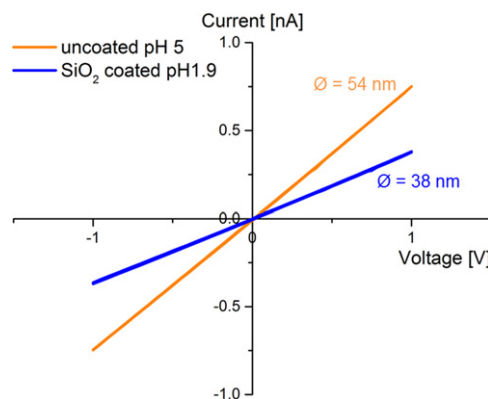
Figure 5. Detailed XP spectra of nominal 10 nm thick layers of (a) TiO$_2$, (b) SiO$_2$ [36], and (c) Al$_2$O$_3$. The corresponding binding energies are indicated by vertical dashed lines.
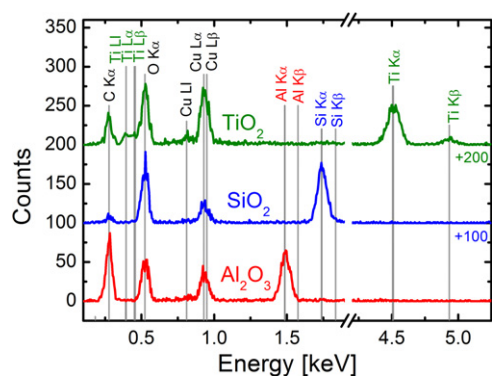
Figure 6. Integrated EDX spectra recorded from linescans across single TiO$_2$ (green), SiO$_2$ (blue), and Al$_2$O$_3$ (red) nanotubes (outer diameter ∼50 nm, wall thickness ∼20 nm). The copper and carbon signals are ascribed to contributions from the Cu-lacey TEM grids.

Figure 7. *I–V* curve of a single, cylindrical nanochannel in a 30 *μ*m thick PC membrane before (orange) and after (blue) ALD coating. After coating with a nominal thickness of 10 nm SiO$_2$, the initial diameter decreased from ∼54 to ∼38 nm. Ohmic *I–V* curves were measured at the electrolyte pH corresponding to the isoelectric point of the wall material.

3.3. Electrolytic characterization of single nanochannel membranes

As demonstrated above, ALD coating provides tailored size reduction of the diameter of nanochannels without affecting the initial channel shape. Controlling this process opens up novel opportunities to precisely adjust the channel dimensions for sensors based on transport processes through single nanopores [4, 53–55]. As proof-of-principle, we recorded ohmic current–voltage (*I–V*) curves on a single-channel membrane before and after ALD coating (figure 7). The

electrolytic conductivity measurements were performed in electrolyte of pH that corresponds to the isoelectric point of the wall material (pH 5 for the uncoated channel and pH 1.9 fot the SiO$_2$-coated channel). The channel diameter as determined from the conductivity data (equation given in section 2.6) is ∼54 nm before coating, in agreement with the etching rate measured for a multichannel reference membrane. After deposition of 56 cycles SiO$_2$, the *I–V* curve of the same nanochannel membrane yielded a deduced diameter of

~38 nm. This diameter reduction coincides well with the nominal coating thickness and the reference multichannel sample.

This experiment clearly exhibits successful ALD coating of a single cylindrical nanochannel and the corresponding reduced ion transport due to the smaller channel diameter.

4. Conclusions

The combination of ion-track technology and ALD provides unique opportunities for highly homogeneous and conformal coatings of extremely long nanochannels without affecting their initial geometry. Our results clearly demonstrate successful conformal coating of cylindrical 30 μm long nanochannels with initial diameter between 55 and 18 nm by three different inorganic materials (TiO$_2$, SiO$_2$, and Al$_2$O$_3$). Although the ALD process presents great flexibility with respect to the deposited material, the chemical process had to be adjusted to temperatures low enough to avoid damage to the ion-track etched polymer membranes.

XPS on film surfaces as well as EDX analysis of single nanotubes evidenced homogeneous near-stoichiometric TiO$_2$, SiO$_2$, and Al$_2$O$_3$ layers. Inside the nanochannels the deposition of TiO$_2$ and SiO$_2$ follows nearly the same layer-by-layer growth mechanism as for flat macroscopic surfaces. For Al$_2$O$_3$, the applied process needs further optimization. TiO$_2$, SiO$_2$, and Al$_2$O$_3$ nanotubes released from the PC membrane represent stable nanostructures with walls as thin as 10 nm and aspect ratios as high as 3000.

Ionic transport measurements of single-nanochannel membranes coated with SiO$_2$ yield promising results. ALD allows fine-tuning of surface properties and controlled shrinking of the size of single nanopores, thus providing well-defined nanoconfinements with tailored inorganic surfaces for future transport studies.

Acknowledgments

References

[1] Siwy Z, Gu Y, Spohr H A, Baur D, Wolf-Reber A, Spohr R, Apel P and Korchev Y E 2002 Rectification and voltage gating of ion currents in a nanofabricated pore *Europhys. Lett.* **60** 349–55

[2] Siwy Z, Apel P, Baur D, Dobrev D D, Korchev Y E, Neumann R, Spohr R, Trautmann C and Voss K-O 2003 Preparation of synthetic nanopores with transport properties analogous to biological channels *Surf. Sci.* **532-535** 1061–6

[3] Heins E A, Siwy Z S, Baker L A and Martin C R 2005 Detecting single porphyrin molecules in a conically shaped synthetic nanopore *Nano Lett.* **5** 1824–9

[4] Ali M, Yameen B, Neumann R, Ensinger W, Knoll W and Azzaroni O 2008 Biosensing and supramolecular bioconjugation in single conical polymer nanochannels. Facile incorporation of biorecognition elements into nanoconfined geometries *J. Am. Chem. Soc.* **130** 16351–7

[5] Schiedt B, Healy K, Morrison A P, Neumann R and Siwy Z 2005 Transport of ions and biomolecules through single asymmetric nanopores in polymer films *Nucl. Instrum. Methods Phys. Res.* B **236** 109–16

[6] Pevarnik M, Healy K, Toimil-Molares M E, Morrison A, Létant S E and Siwy Z S 2012 Polystyrene particles reveal pore substructure as they translocate *ACS Nano* **6** 7295–302

[7] Innes L M, Chen C-H, Schiel M, Pevarnik M, Haurais F, Toimil-Molares M E, Vlassiouk I, Theogarajan L and Siwy Z S 2014 Velocity profiles in pores with undulating opening diameter and their importance for resistive-pulse experiments *Anal. Chem.* **86** 10445–53

[8] Sattig M, Reutter S, Fujara F, Werner M, Buntkowsky G and Vogel M 2014 NMR studies on the temperature-dependent dynamics of confined water *Phys. Chem. Chem. Phys.* **16** 19229–40

[9] VanDersarl J J, Xu A M and Melosh N A 2012 Nanostraws for direct fluidic intracellular access *Nano Lett.* **12** 3881–6

[10] Healy K, Schiedt B and Morrison A P 2007 Solid-state nanopore technologies for nanopore-based DNA analysis *Nanomedicine.* **2** 875–97

[11] Chen P, Mitsui T, Farmer D B, Golovchenko J, Gordon R G and Branton D 2004 Atomic layer deposition to fine-tune the surface properties and diameters of fabricated nanopores *Nano Lett.* **4** 1333–7

[12] Kelly D N, Wakabayashi R H and Stacy A M 2014 A Modified sol–gel technique for pore size control in porous aluminum oxide nanowire templates *ACS Appl. Mater. Interfaces* **6** 20122–9

[13] Storm A J, Chen J H, Ling X S, Zandbergen H W and Dekker C 2003 Fabrication of solid-state nanopores with single-nanometre precision *Nat. Mater.* **2** 537–40

[14] Fleischer R L 1975 *Nuclear Tracks in Solids: Principles and Applications* (Berkeley, CA: University of California Press)

[15] Steckenreiter T, Balanzat E, Fuess H and Trautmann C 1999 Pyrolytic effects induced by energetic ions in polymers *Nucl. Instrum. Methods Phys. Res.* B **151** 161–8

[16] Cornelius T W, Apel P Y, Schiedt B, Trautmann C, Toimil-Molares M E, Karim S and Neumann R 2007 Investigation of nanopore evolution in ion track-etched polycarbonate membranes *Nucl. Instrum. Methods Phys. Res.* B **265** 553–7

[17] Toulemonde M, Trautmann C, Balanzat E, Hjort K and Weidinger A 2004 Track formation and fabrication of nanostructures with MeV-ion beams *Nucl. Instrum. Methods Phys. Res.* B **216** 1–8

[18] Fischer B E 1988 The heavy-ion microprobe at GSI—used for single ion micromechanics *Nucl. Instrum. Methods Phys. Res.* B **30** 284–8

[19] Apel P Y and Dmitriev S N 2011 Micro- and nanoporous materials produced using accelerated heavy ion beams *Adv. Nat. Sci.: Nanosci. Nanotechnol.* **2** 013002

[20] Spohr R 2005 Status of ion track technology—prospects of single tracks *Radiat. Meas.* **40** 191–202

[21] Trautmann C 2009 Micro- and nanoengineering with ion tracks *Ion Beams in Nanoscience and Technology* ed R Hellborg *et al* (Berlin: Springer) pp 369–87

[22] Toimil-Molares M E 2012 Characterization and properties of micro- and nanowires of controlled size, composition, and geometry fabricated by electrodeposition and ion-track technology *Beilstein J. Nanotechnol.* **3** 860–83

[23] Kohli P, Wharton J E, Braide O and Martin C R 2004 Template synthesis of gold nanotubes in an anodic alumina membrane *J. Nanosci. Nanotechnol.* **4** 605–10

[24] Muench F, Kunz U, Neetzel C, Lauterbach S, Kleebe H-J and Ensinger W 2011 4-(Dimethylamino)pyridine as a powerful auxiliary reagent in the electroless synthesis of gold nanotubes *Langmuir* **27** 430–5

[25] Wolf-Reber A 2002 *PhD Thesis* Universität Frankfurt

[26] Sander M S, Côté M J, Gu W, Kile B M and Tripp C P 2004 Template-assisted fabrication of dense, aligned arrays of titania nanotubes with well-controlled dimensions on substrates *Adv. Mater.* **16** 2052–7

[27] Elam J W, Routkevitch D, Mardilovich P P and George S M 2003 Conformal coating on ultrahigh-aspect-ratio nanopores of anodic alumina by atomic layer deposition *Chem. Mater.* **15** 3507–17

[28] Romero V, Vega V, García J, Zierold R, Nielsch K, Prida V M, Hernando B and Benavente J 2013 Changes in morphology and ionic transport induced by ALD SiO₂ coating of nanoporous alumina membranes *ACS Appl. Mater. Interfaces* **5** 3556–64

[29] George S M 2010 Atomic layer deposition: an overview *Chem. Rev.* **110** 111–31

[30] Chang Y-H, Liu C-M, Cheng H-E and Chen C 2013 Effect of geometric nanostructures on the absorption edges of 1D and 2D TiO₂ fabricated by atomic layer deposition *ACS Appl. Mater. Interfaces* **5** 3549–55

[31] Shin H, Jeong D-K, Lee J, Sung M M and Kim J 2004 Formation of TiO₂ and ZrO₂ nanotubes using atomic layer deposition with ultraprecise control of the wall thickness *Adv. Mater.* **16** 1197–200

[32] Jeong D, Lee J, Shin H, Lee J, Kim J and Sung M 2004 Synthesis of metal-oxide nanotubular structures by using atomic layer deposition on nanotemplates *J. Korean Phys. Soc.* **45** 1249–52

[33] Bae C, Kim S, Ahn B, Kim J, Sung M M and Shin H 2008 Template-directed gas-phase fabrication of oxide nanotubes *J. Mater. Chem.* **18** 1362

[34] Triani G, Evans P J, Attard D J, Prince K E, Bartlett J, Tan S and Burford R P 2006 Nanostructured TiO2 membranes by atomic layer deposition *J. Mater. Chem.* **16** 1355

[35] Abou Chaaya A *et al* 2013 Enhanced ionic transport mechanism by gramicidin a confined inside nanopores tuned by atomic layer deposition *J. Phys. Chem.* C **117** 15306–15

[36] Sobel N, Hess C, Lukas M, Spende A, Stühn B, Toimil-Molares M E and Trautmann C 2015 Conformal SiO₂ coating of sub-100 nm diameter channels of polycarbonate etched ion-track channels by atomic layer deposition *Beilstein J. Nanotechnol.* **6** 472–9

[37] Ferain E and Legras R 1994 *Nucl. Instrum. Methods Phys. Res.* B **84** 331–6

[38] Apel P Y, Blonskaya I V, Dmitriev S N, Orelovitch O L, Presz A and Sartowska B A 2007 Fabrication of nanopores in polymer foils with surfactant-controlled longitudinal profiles *Nanotechnology* **18** 305302

[39] Cornelius T W, Schiedt B, Severin D, Pépy G, Toulemonde M, Apel P Y, Boesecke P and Trautmann C 2010 Nanopores in track-etched polymer membranes characterized by small-angle x-ray scattering *Nanotechnology* **21** 155702

[40] Zhu Z, Maekawa Y, Liu Q and Yoshida M 2005 Influence of UV light illumination on latent track structure in PET *Nucl. Instrum. Methods Phys. Res* B **236** 61–7

[41] Kubrin R, Lee H S, Zierold R, Yu Petrov A, Janssen R, Nielsch K, Eich M and Schneider G A 2012 Stacking of ceramic inverse opals with different lattice constants ed J Ballato *J. Am. Ceram. Soc.* **95** 2226–35

[42] Lee H S, Kubrin R, Zierold R, Petrov A Y, Nielsch K, Schneider G A and Eich M 2013 Photonic properties of titania inverse opal heterostructures *Opt. Mater. Express* **3** 1007

[43] Du Y, Du X and George S M 2005 SiO₂ film growth at low temperatures by catalyzed atomic layer deposition in a viscous flow reactor *Thin Solid Films* **491** 43–53

[44] Rahtu A and Ritala M 2002 Reaction mechanism studies on titanium isopropoxide–water atomic layer deposition process *Chem. Vapor Depos.* **8** 21

[45] Klaus J W, Ofer S and George S M 1997 Growth of SiO₂ at room temperature with the use of catalyzed sequential half-reactions *Science* **278** 1934–6

[46] Engel M, Stühn B, Schneider J J, Cornelius T and Naumann M 2009 Small-angle x-ray scattering (SAXS) off parallel, cylindrical, well-defined nanopores: from random pore distribution to highly ordered samples *Appl. Phys.* A **97** 99–108

[47] Kuttich B, Engel M, Trautmann C and Stühn B 2014 Tailored nanochannels of nearly cylindrical geometry analysed by small angle x-ray scattering *Appl. Phys.* A **114** 387–92

[48] Mayer J T, Diebold U, Madey T E and Garfunkel E 1995 Titanium and reduced titania overlayers on titanium dioxide (110) *J. Electron Spectrosc. Relat. Phenom.* **73** 1–11

[49] Wu C-Y, Lee Y-L, Lo Y-S, Lin C-J and Wu C-H 2013 Thickness-dependent photocatalytic performance of nanocrystalline TiO₂ thin films prepared by sol–gel spin coating *Appl. Surf. Sci.* **280** 737–44

[50] Himpsel F, McFeely F, Taleb-Ibrahimi A, Yarmoff J and Hollinger G 1988 Microscopic structure of the SiO₂/Si interface *Phys. Rev.* B **38** 6084–96

[51] Wilson C A, Grubbs R K and George S M 2005 Nucleation and growth during Al₂O₃ atomic layer deposition on polymers *Chem. Mater.* **17** 5625–34

[52] Kim J, Chakrabarti K, Lee J, Oh K-Y and Lee C 2003 Effects of ozone as an oxygen source on the properties of the Al₂O₃ thin films prepared by atomic layer deposition *Mater. Chem. Phys.* **78** 733–8

[53] Davenport M, Rodriguez A, Shea K J and Siwy Z S 2009 Squeezing ionic liquids through nanopores *Nano Lett.* **9** 2125–8

[54] Ali M, Ramirez P, Mafé S, Neumann R and Ensinger W 2009 A pH-tunable nanofluidic diode with a broad range of rectifying properties *ACS Nano* **3** 603–8

[55] Ali M, Schiedt B, Healy K, Neumann R and Ensinger W 2008 Modifying the surface charge of single track-etched conical nanopores in polyimide *Nanotechnology* **19** 085713